This is an Accepted Manuscript of the article **Curcoll, R., Camarero, L., Bacardit, M., Àgueda, A., Grossi, C., Gacia, E., ... & Morguí, J. A. (2019). Atmospheric Carbon Dioxide variability at Aigüestortes, Central Pyrenees, Spain. *Regional Environmental Change*, 1-12** , available online at: https://doi.org/10.1007/s10113-018-1443-2

Atmospheric Carbon Dioxide at Aigüestortes, Central Pyrenees, Spain

Authors:
Roger Curcoll[1,2,7,8,*]
Lluís Camarero[3,7] (camarero@ceab.csic.es)
Montse Bacardit[4] (m.bacardit@aran.org)
Alba Àgueda[1,8] (alba.agueda@upc.edu)
Claudia Grossi[1,9,10] (claudia.grossi@upc.edu)
Esperança Gacia[3,7] (gacia@ceab.csic.es)
Anna Font[5] (anna.font_font@kcl.ac.uk)
Josep-Anton Morguí[1,2,6,7] (JosepAnton.Morgui@uab.cat)

1: Institut Català de Ciències del Clima, IC3, Spain
2: Institut de Ciència i Tecnologia Ambientals, ICTA-UAB, Spain
3: Centre d'Estudis Avançats de Blanes, CEAB-CSIC, Spain
4: Centre de Lauegi, Conselh Generau d'Aran, Spain
5: Environmental Research Group, MRC PHE Centre for Environment and Health, King's College London, United Kingdom
6: Departament de Biologia Evolutiva, Ecologia i Ciències Ambientals (BEECA), UB, Spain
7: Associació LTER-Aigüestortes, Spain
8: Departament d'Enginyeria Química, Universitat Politècnica de Catalunya (UPC), Spain
9: Institut de Tècniques Energètiques (INTE), UPC, Spain
10: Departament de Fisica Nuclear, UPC, Spain

* corresponding author.
E-mail: roger.curcoll@uab.cat
Address: ICTA-ICP Building Z Campus UAB, 08193 Bellaterra (Cerdanyola) · Barcelona, Spain
Phone number: +34 665833653

Keywords
CO_2, Mountain Site, LTER, Long-Term Ecological Research, Atmospheric measurements, Pyrenees

Abstract

In order to improve the understanding of the carbon cycle in the Pyrenean region two atmospheric monitoring mountain stations were set up within the Long-Term Ecological Research node of Aigüestortes i Estany de Sant Maurici at Central Pyrenees, Spain. The atmospheric concentration of carbon dioxide (CO_2) was measured over 2008-2014 and 2010-2014 at Estany Llong site (ELL) and Centre de Recerca d'Alta Muntanya (CRAM), respectively. Measurements were carried out fortnightly off-line with high precision instrumentation at ELL and every minute on-line with a lower precision sensor at CRAM in conjunction with meteorological variables. The two data sets were analyzed in this study, quantifying whenever possible annual growth rates (AGR), seasonal variability and diurnal amplitudes. Results were also compared with the NOAA Marine Boundary Layer (MBL) reference product and CO_2 data from other background monitoring stations. Four-harmonics adjusted CO_2 data from ELL showed a high correlation with the NOAA MBL reference product for the same latitude (Spearman's rho ρ=0.96). In addition, AGRs of CO_2 at ELL correlated well with those observed at Mace Head (MHD) station (ρ=0.94), suggesting that ELL can be considered a background station. Winter CRAM CO_2 data was not statistically different from ELL data, while in summer it was 5.5 ppm lower on average, suggesting a higher photosynthesis uptake. The amplitude of the CO_2 diurnal cycle at

CRAM was found to be exponentially related to the local mean daily temperature and dependent on forthcoming wind sector (N-NW or E-SE-S-SW). An increase in CRAM CO_2 concentrations was observed under N-NW winds during daytime, which could be related to traffic emissions. This study demonstrates that the use of CO_2 sensors with low precision but continuously corrected and periodically calibrated can be used for the study of local and regional CO_2 sources and sinks.

1. Introduction

Accurate assessment of CO_2 emissions and their redistribution among the atmosphere, ocean, and terrestrial biosphere is important to better understand the global carbon cycle, to support the development of climate policies and to mitigate and tackle climate change (Bouwman 1989; Post et al. 1990; Tans et al. 1990a; Le Quéré et al. 2016).

The distribution of CO_2 sources and sinks are poorly constrained at regional (10^2–10^6 km^2) and seasonal scales (Ciais et al. 2000; Geels et al. 2007; Bergamaschi et al. 2010; Hase et al. 2015; Hu et al. 2018). Top-down techniques are useful to estimate carbon fluxes from atmospheric CO_2 observations (Ciais et al. 2010). These top-down inversion models are more consistent for regions where the atmospheric network is dense (Peylin et al. 2013). Unfortunately, the number of measurements and their spatial coverage are still insufficient in some European regions such as the NW of the Mediterranean (Marquis and Tans 2008).

Remote mountain stations, located far away from anthropogenic sources, can provide useful information to investigate trends of large-scale background levels (Ciattaglia et al. 1987; Colombo et al. 2000; Schmidt 2003; Schibig et al. 2015; Bamberger et al. 2017). When local influences are filtered, mountain greenhouse gases (GHGs) time series can be considered suitable for global inversion models (Levin 1987; Bamberger et al. 2017). Monitoring GHGs in mountainous remote sites is also useful to understand the variability of the response of the mountain ecosystems to global warming (e.g. Randerson et al. 1999; Bakwin et al. 2004; Angert et al. 2005). Moreover, when the inversion models focus on small scales and utilize continental measurements of CO_2 they can better resolve the responses of various vegetation types and the impact of human interventions on land-atmosphere fluxes (Pillai et al. 2011).

In order to supply to the lack of CO_2 data in the NW Mediterranean region, atmospheric measurements were carried out since 2008 at Estany Llong (ELL), a mountain site in Central Pyrenees (north Spain). In 2010 continuous CO_2 measurements started at the nearby site of CRAM (Centre de Recerca d'Alta Muntanya). The two sites are part of the Long-Term Ecological Research (LTER) node of the 'Aigüestortes i Estany de Sant Maurici National Park' (ANP). The ANP has been a node of scientific research for hydrology (Catalan 1989), atmospheric chemistry (Bacardit and Camarero 2009; Curcoll et al. 2010; Camarero et al. 2017), atmospheric biology (Hervàs et al. 2009), biogeochemistry of surface waters (Camarero and Catalan 1993), aquatic organisms (Chappuis et al. 2011; 2014) and terrestrial flora and fauna (Carrillo and Ninot 1992).

The present study aims to assess the suitability of two Central Pyrenees GHGs atmospheric stations for regional-scale CO_2 monitoring and to evaluate the influencing factors driving the observed CO_2 variability at different temporal scales. More specifically, in this study ELL and CRAM CO_2 time series are presented for the first time and they are statistically analyzed with two specific goals: i) To offer the data to the scientific community and discuss their spatial representativeness; ii) To determine the sources of variability and to differentiate anthropogenic from natural influences.

After a short description of the sites, the sampling and analyzing methodology is addressed, remarking the precision and accuracy of the analytical procedure. Daily, monthly and annual variabilities of the two data sets are examined whenever possible, depending on their temporal resolution. To better interpret our results, we compare the obtained annual growth rates and seasonal variabilities with those from other European sites (Monte Cimone - Italy, Mace Head – UK, and CIBA – Spain). We also examine the influence of wind direction and ambient temperature. Finally, we use the results of these two sites (ELL and CRAM) to discuss whether the use of low-precision sensors can be justified in areas with low maintenance requirements.

2. Methods

2.1 Sites description

In 2008 LTER-Aigüestortes node was established as a member of the LTER-Spain network (Camarero and Morguí 2009). In the same year, a continuous atmospheric CO_2 monitoring program was established at

the eastern extreme of Estany Llong Lake (ELL). The remote sampling site of ELL (42.57N, 0.95E, 2,003 meters above sea level [m asl]) is located inside the ANP. The ANP (14,119 ha) and its peripheral protection area (26,733 ha) are located in the southern axial chain of the Central Pyrenees, in northeastern Spain. It is a high-mountain area and its altitude ranges between 1,383 and 3,029 m asl. The climate is Atlantic mountain-type (Albentosa Sánchez 1973), with strong winters and snow present from November to May. Precipitation presents annual accumulated values of 1,200-1,300 mm. The annual mean temperature is 5.2ºC with the highest monthly average in July (19.3ºC) and the lowest in February (-4.3ºC) (Ninyerola et al. 2003). The location is actually a mountain meadow of *Festuca sp*. and *Nardus sp*. surrounded by granite mountains and coniferous forest (Carreras and Diego 2007). Valley and mountain breezes are common at this site with upslope winds during the day and downslope breezes at night (Camarero et al. 2018).

In 2010, continuous atmospheric CO_2 measurements started at CRAM (42.62N, 0.77E, 1,584 m asl). The CRAM is located at the top of the Noguera Ribagorçana valley that has a North-South orientation. The valley is located 16 km west of the ELL remote site, in the peripheral area of the ANP. The CRAM station is located 200 meters south of the Vielha road tunnel entrance (5,230 m long). It is surrounded by grassland in the North and mixed, deciduous and coniferous forests in the South (Carreras and Diego 2007). A map with the location of both sites with Corine land cover cartography can be found in the support material (Figure S1).

2.2 Estany Llong sampling and analytical method

Fortnightly samplings were carried out at ELL since April 2008. Samples were collected in two 1L cylindrical borosilicate glass flasks (Normag Labor und Prozesstechnik GmbH, Germany) with Kel-F PCTFE valves fitted at both ends. This material shows the lowest permeation of gases compared to other sealing materials (Sturm et al. 2004). Flasks were sampled using a new developed self-made sampling device suitable for remote sites. Air was taken at 3.5 meters above ground level (m agl) and was dried by passing through a desiccant (magnesium perchlorate). Then the sampled air was filtered to remove particles and pumped to the flasks. Air was flushed through a pair of flasks for at least 10 minutes at a flow rate between 2.0 and 3.5 l min^{-1}. After, the exit valve was closed and flasks were pressurized with sampled air up to 1.5 bargs. Air samples were collected between 10 and 12 GMT, when the mixed boundary layer was developed and the valley breeze established. These previous conditions were selected to sample the widest possible influence area. Air temperature, relative humidity, atmospheric pressure and wind direction and speed were measured using a portable Kestrel 5500 weather device during ELL flasks sampling. According to factory specifications, accuracy of the instrument is 0.5ºC (temperature), 2% (relative humidity), 1.5 mbar (pressure), 5º (wind direction) and 3% (wind speed).

Flasks samples from ELL site were analyzed for CO_2 using two differential, non-dispersive infrared gas analyzers (Licor7000) in series. Each Licor7000 had two cells and two detectors for a simultaneous measurement of CO_2 and H_2O vapor on a reference and a sample stream. A vacuum pump was installed to empty the backspace between the flask valve and the analyzer inlet. A sketch of the analyzing instrumental configuration can be found in the support material (Figure S2). Both sample and reference were flushed through the cells at a flow rate of 0.1 l min^{-1} controlled by two Bronkhorst mass flow controllers. On the sample line, a Valco multivalve was used to switch between calibration standards, samples and reference gas. Reference gas passed through the sample cell before and after each flask analysis. The value of the reference gas in the sample cell was used as a baseline to cope with instrument drift.

The Licor7000 has a strong dependency on cell pressure and temperature (Gomez-Pelaez and Ramos 2011). To minimize the pressure influence, both Licor7000 were modified and the pressure sensors were removed and two additional Bronkhorst backpressure controllers at the end of the reference and sample lines were installed to keep the pressure stable inside the cells. Since 2010, the room temperature in the laboratory was controlled with a specific air-conditioning equipment keeping the temperature stable at 23 ± 0.3ºC. In 2013 both Licor7000 analyzers were installed in a Boxcult box and the cell temperature of instruments was stabilized at 30 ± 0.1ºC. Improvements made on temperature control reduced the error and the drift of both analyzers. Average absolute difference between CO_2 calibrated measures of both analyzers decreased through the years, being 0.104 ppm in the 2008-2009 period, 0.041 in 2010-2012 and 0.029 in 2013-2015. The CO_2 values used in this study are the mean calculated from both analyzers. The use of the two Licor7000 analyzers in series improved the precision of the measurement and was useful for tracking instruments drift.

Each day that a set of flasks had to be analyzed in the lab, the two Licor7000 were calibrated every 4 hours with four secondary standards cylinders. These secondary standards were recalibrated every six months with 6 NOAA standards (WMO X2007 scale; Zhao and Tans 2006). Each flask was analyzed for seven minutes, time that best compromised the stability of the measurements and the lack of flow and pressure drop. For each measurement, only the last 30 seconds were considered for calculation. The two flasks of each sampling were analyzed on different days to cope with the instrument variability and differences due to calibrations. Uncertainties in the measured concentrations stemmed from both the sampling method and the analysis (Tans et al. 1990b). Pairs of flasks that had a difference higher than 0.7 ppm of CO_2 between both calibrated values were discarded. The average differences between the two flasks of each pair was -0.03 (1σ: ± 0.3) ppm. This deviation was consistent with other CO_2 flask measurements (e.g. Conway et al. 1994; Andrews et al. 2014).

2.3. Continuous sampling at the Centre de Recerca d'Alta Muntanya site

A Vaisala GMP343 carbon dioxide probe was installed for continuous CO_2 measurements in 2010 at CRAM station. Air inlet was at 3 m agl and the probe was protected from direct radiation and rain. The GMP343 sensor is an infrared absorbance CO_2 detector that uses a micromachined electrically tunable Fabry-Perot Interferometer (FPI). The FPI enables a reference measurement at a wavelength where no absorption occurs to improve the measurement (Vaisala 2017). The GMP343 has been used in atmospheric and biospheric studies where very high precision is not required (Pumpanen et al. 2008; Rigby et al. 2008). Factory precision of the instrument was 1% with a minimum long-term drift of ± 10 ppm CO_2 $year^{-1}$. A Vantage Pro2 Davis weather station that delivered temperature, pressure, relative humidity and wind direction and wind speed data was also installed at CRAM. The GMP343 has an internal correction algorithm that considers temperature, humidity and pressure. Pressure and relative humidity from the meteorological station were sent to the instrument via RS232 every 10 minutes to correct CO_2 data. Correction for temperature was made using the internal GMP343 temperature sensor.

The instrument was calibrated at least twice a year by comparing concentrations with a collocated Picarro G2301 Cavity RingDown Spectroscopy Analyzer (CRDS), this latter with a precision better than 0.03 ppm for CO_2 (Crosson 2008; Richardson et al. 2012). In the intercomparison events, the G2301 analyzer was collocated for at least one week. G2301 results were corrected for water vapor (Rella et al. 2013) and further calibrated in the laboratory using six NOAA reference gases before and after each intercomparison. Residuals of the linear fit between CO_2 values measured by GMP343 and CO_2 values measured by G2301 showed a strong dependence on temperature. Therefore, an additional correction for temperature was implemented. The final CO_2 concentrations measured by GMP343 were obtained by linear regression of measured CO_2 and temperature as expressed in Equation 1, where T_{GMP} is the temperature measured by the GMP343, $CO_{2(GMP)}$ is the value of the GMP343 and $CO_{2(corr)}$ the corrected CO_2 value, measured by the G2301 analyzer. After applying the additional temperature correction, Residual Standard Error (RSE) for CO_2 calibration events was 1.5 ppm (1 week).

(1) $$CO_{2(corr)} = A + B \cdot CO_{2(GMP)} + C \cdot T_{GMP}$$

A strong linear drift was observed on GMP343 data between calibrations (~ 15 ppm $year^{-1}$), probably caused by the soiling of the mirrors of the sensor. A linear scaling was applied to CO_2 time series to correct for drift.

2.5 Data analysis

2.5.1. CO_2 time series curve fitting

The Carbon Cycle Group CuRVe (CCGCRV) is a digital time series filtering algorithm developed by Kirk Thoning within the Carbon Cycle Group, Earth System Research Laboratory at NOAA (USA) in the late 1980s (Thoning et al. 1989). Approximations of the seasonal cycle and the long-term trend are made by fitting a polynomial equation combined with a harmonic function. CCGCRV fit is recommended for analysis of time series where it is important to accurately represent the magnitude of the seasonal cycle or the timing of the seasonal inflexion points and for analyses where the year-to-year variation in the seasonal and trend

components are retained (Pickers and Manning 2015). We have applied the CCGCRV to the ELL CO_2 series using the recommended parameters by Pickers and Manning (2015): number of yearly harmonics = 4, number of polynomial terms = 3, short-term cutoff = 50 days, long-term cutoff = 667 days.

2.5.2. Bivariate Polar Plots for wind sectors analysis

The location of potential local sources and sinks at both ELL and CRAM was explored through bivariate polar plots (Carslaw and Ropkins 2012). The ELL bivariate polar plot was composed with the residuals of the ELL CO_2 series from the 4-harmonics CCGCRV fit curve instead of using the actual concentrations. By doing so we remove the seasonal and the inter-annual variabilities. For the CRAM data set bivariate polar plots for absolute CO_2 concentrations were generated.

2.5.3. Ambient temperature influence on the diurnal amplitude.

Due to the measurement error of the GMP343 sensors being greater than 1 ppm, the time series at CRAM was only used for the analysis of large CO_2 variations (diurnal and seasonal cycles) but not for the study of long-term trends. Meteorological variables from the Davis station were also used. Hourly means were calculated from minute measurements. For all the measurement days at CRAM, the amplitude of the CO_2 diurnal cycle was calculated as the difference between the daily maximum concentration and the daily minimum.

To evaluate the influence of air temperature on the diurnal CO_2 cycle, the Lloyd and Taylor formulation was used. It is a semi-empirical formulation that relates the temperature dependency of soil respiration, reflecting the decrease in the respiration activation energy with increasing temperature (Lloyd and Taylor 1994) (Equation 2). Although this equation was formulated for soil respiration (R, μmol C m^{-2} s^{-1}), we consider that the amplitude of the CO_2 diurnal cycle at CRAM is dependent on the soil respiration and ecosystem photosynthesis, both controlled by temperature (Berry and Bjorkman 1980; Smith and Dukes 2013). Therefore, in our approximation the variable R refers to the amplitude of the diurnal cycle (ppm CO_2).

(2) $$R = Ae^{\frac{-E_0}{T-T_0}}$$

While the regression parameter T_0 is kept constant at -46.02 ºC (Lloyd and Taylor 1994), the activation energy kind of parameter (E_0) is a free parameter that sets the temperature sensitivity (Reichstein et al. 2005). T is the average diurnal temperature and A is a dataset dependent variable.

2.5.4. Data retrieval from NOAA Marine Boundary Layer, background monitoring stations and global flux models for data comparison

ELL CO_2 time series were compared with the NOAA CO_2 Marine Boundary Layer (MBL) reference product for the same latitude (Dlugokencky et al. 2017b). The NOAA MBL reference product is derived directly from measurements of weekly air samples and gives low-noise representation of the annual variability and the ongoing global increase of CO_2 (Masarie and Tans 1995). The zonal product of the NOAA MBL gives the marine background concentration for a range of latitudes (42.57-42.58 degrees north in our case). Each value has an associated uncertainty assigned by the density of measurements on a given period. The average associated error for the 2008-2014 period was 0.61 ppm. The CCGCRV curve was also applied to the MBL data series for a better statistical analysis.

To evaluate ELL as a mountain site capturing long-term changes we have retrieved data from nearby stations that measure CO_2 with weekly flask measurements. Selected stations were: (1) Monte Cimone (CMN; 44.18N, 10.70E, 2,165 m asl), a mountain station at similar latitude and altitude (Ciattaglia 1983; Ciattaglia et al. 1987; Cundari et al. 1990; Cundari et al. 1995; Cristofanelli et al. 2018); (2) Mace Head (MHD, 53.33N, 9.90W, 5 m asl), located in the west Atlantic coast of Ireland and considered in many studies as a reference for Europe (Conway et al. 1994; Dlugokencky et al. 2017); (3) CIBA (CIB, 41.81N, 4.93W, 856 m asl), a northern-Spain station located in an agricultural area at a similar latitude as ELL (Sánchez et al. 2010; Dlugokencky et al. 2017). Data from these stations have been obtained via NOAA ObsPack products (Cooperative Global Atmospheric Data Integration Project 2013, 2017). The growth rate for these stations was also obtained using the CCGCRV algorithm.

Modeled values of annual terrestrial flux from two global models, MACC-V2 (Chevallier et al. 2010) and JENA-MPI (Rödenbeck et al. 2003), were obtained from the Global Carbon Atlas (http://www.globalcarbonatlas.org/en/flux-time-series).

3. Results

3.1 Estany Llong data series results

3.1.1 Estany Llong annual growth rates.

The CCGCRV analysis was applied at ELL CO_2 data series with a good agreement (Residual Standard Error = 1.71 ppm) (Figure 1). Signals of strong systematic anthropogenic or natural influences of samples seem not to be present in the ELL CO_2 data series. When comparing the harmonic function of ELL with the MBL reference, annual cycle of both series had a similar pattern and amplitude, with a slightly earlier spring decrease of the CO_2 concentration at ELL. The non-parametric Spearman's rank coefficient was used to analyze the correlation between series. Spearman's rho (ρ) correlation between the two whole series was 0.96 and ELL CO_2 concentrations were 0.89 ± 1.57 (1σ) ppm lower than the MBL reference over the period 2008-2013. Thus, the two time series do not differ. Moreover we must take into account the average associated error for the NOAA MBL series, 0.61 ppm (Dlugokencky et al. 2017b). This result suggests that ELL is mainly capturing a background signal.

From the 4-harmonic function, the annual growth was obtained. The variability in the annual growth rate of both ELL and NOAA MBL CO_2 series followed a similar tendency (ρ=0.77), with the highest value in 2010 (2.76 and 3.22 ppm CO_2/year respectively); and the lowest in 2009 for ELL (1.11 ppm) and in 2011 for NOAA MBL (1.48 ppm CO_2/year). Average annual growth rate for the period 2008-2013 was 2.18 ± 0.74(1σ) ppm CO_2/year for ELL and 2.20 ± 0.65 (1σ) ppm CO_2/year for NOAA MBL, showing that ELL CO_2 concentrations were growing with a similar trend as for the marine background concentrations (Figure 2).

The highest correlation between annual growth rate at ELL against the other monitoring stations was with Mace Head (ρ=0.94) (Atlantic coastal site) (Figure 2). The other mountain station, Monte Cimone, showed a different behavior, with higher annual variability.

3.1.2 Estany Llong wind direction influence

The windrose for ELL (Figure 3.a) shows that main wind direction followed the valley orientation (NE-E and SW-W). The bivariate polar plot generated from the residuals of the 4-harmonics fitting curve (Figure 3.b) shows that on average there was no difference in CO_2 concentration when the wind blew from the valley (SW-W) or the mountain top (NE-E). Other forthcoming directions showed higher (SE) and lower (NW) signals, but the amount of data was too scarce to generate consistent conclusions.

3.2 Centre de Recerca d'Alta Muntanya data series results

3.2.1 Centre de Recerca d'Alta Muntanya diurnal cycle

The diurnal cycle of CO_2 concentration at CRAM shows a significant variability depending on the season (Figure S3). The highest daily maximum concentration was measured in February and the lowest in August. In summer, when ecosystem respiration and photosynthesis at northern mid-latitudes get the maximum rates (Potter and Randerson 1993), the diurnal amplitude was higher, with average values of 31.4 ± 10.5 (1σ) ppm. In winter months, the average diurnal amplitude was reduced to 7.5 ± 4.5 (1σ) ppm. The average amplitude of the annual cycle of daily means in CRAM was 9.1 ppm.

3.2.2. Centre de Recerca d'Alta Muntanya wind direction influence

The influence of the air masses origin in the CRAM CO_2 concentration is shown in a bivariate polar plot in Figure 4a. The non-parametric Mann-Whitney-Wilcoxon test was used to statistically find the differences between the CO_2 concentrations from the different sectors. An average difference of 4.7 ppm was found between N-NW and E-SE-S-SW winds for the period 2011-2013 [95% Confidence Interval (CI): 4.1 to 5.3, $p<10^{-15}$] (Figure 4a). The observed differences were magnified in daytime, when the photosynthetic activity is higher, the up-valley wind is more frequent, and the transit of vehicles is higher (4.9 ppm, 4.3 to 5.3 CI, $p<10^{-15}$) (Figure 4b). In nighttime, when traffic was significantly reduced, the CO_2 concentrations were mostly driven by respiration processes and the accumulation in the lower boundary layer and there was no significant difference between the concentrations of the two directions ($p>0.5$) (Figure 4c). These differences

in concentration between N-NW and E-SE-S-SW winds were also greater in summer (5.0 ppm, 4.5 to 5.5 CI, $p<10^{-15}$) (Figure 4d), when photosynthetic processes decreased CO_2 concentration, and were less significant in winter (1.2 ppm, 0.8 to 1.5 CI, $p<10^{-9}$) (Figure 4e).

3.2.3 Centre de Recerca d'Alta Muntanya temperature influence

The influence of temperature on the diurnal cycle amplitude in the CRAM CO_2 was analyzed. Since up to 20 ppm difference was observed depending on the wind forthcoming direction, data series was split depending on the predominant wind direction over a day: North to North-West sector (N-NW); and East to South-Westerly (E-SE-S-SW). The natural logarithm of the diurnal CO_2 amplitude was plotted against the ambient temperature for both wind sectors and the Lloyd and Taylor equation was used to fit the values (Figure 5). Resulting parameters of Equation 2 are shown in Table 1. The diurnal CO_2 amplitude at the average daily temperature at CRAM (8.1ºC) for both N-NW and E-SE-S-SW wind sectors was 13.3 and 9.0 ppm respectively. The non-parametric Kruskal-Wallis test was used to evaluate if the wind direction was a good explanatory variable of the amplitude of the diurnal cycle. Test result indicated that the diurnal amplitudes for air coming from both sectors were statistically different ($p<10^{-15}$). A non-parametric analysis of covariance (Young and Bowman 1995; Bowman and Azzalini 1997) showed that the effect of the temperature on the diurnal cycle was not different for the two wind sectors considered ($p>0.01$). Despite the two wind sectors had different mean amplitudes and were differently influenced by anthropogenic emissions, the effect of temperature on driving the amplitude of the diurnal cycle was the same.

3.3 Seasonal variability of Estany Llong and Centre de Recerca d'Alta Muntanya CO_2 concentration

The mean seasonal variation over 2010-2013 was calculated for ELL and CRAM and also for the other sites (CMN, MHD, CIB and MBL) (Figure 6). Annual maximum at ELL was found in March, and annual minimum in August. ELL annual cycle amplitude was maximum in 2010 (16.2 ppm CO_2) and minimum in 2011 (11.2 ppm CO_2), with an average of 13.2 ± 2.2 (1σ) ppm CO_2.

For CRAM series, only the hours 10-12 GMT were selected for comparison with the ELL CO_2 series. Annual maximum was found in February, a month earlier than ELL, but the annual minimum was also observed in August. Annual cycle amplitude was maximum in 2011 (22.2 ppm CO_2) and minimum in 2013 (19.6 ppm CO_2), with an average of 20.6 ± 1.7 (1σ) ppm.

The Mann-Whitney-Wilcoxon test was used to assess if the mean concentration at ELL and CRAM were statistically different or not. The test was done for winter (DJF) and summer months (JJA). While in summer the mean concentrations at both locations were statistically different ($p<10^{-4}$), winter concentrations were not distinct ($p>0.1$). ELL monthly means were inside the first interquartile range of CRAM data from October to May. In summer both series diverge, being CRAM measurements lower than ELL (5.5 ppm, 3.5 to 7.4 CI).

The highest correlation of the seasonal CO_2 cycle at ELL was observed with the other mountain site, Monte Cimone (ρ=0.84), indicating that both mountain sites behave similarly under seasonal changes (Figure 6). During spring, CRAM and ELL concentrations were similar to the CIBA, located at the same latitude ($p>0.05$). However, CIBA measurements at summertime were extremely variable (σ = 4.6 ppm), causing higher average values (8.9 ppm, 7.6 to 10.3 CI, $p<10^{-15}$). Differences in concentrations for ELL and MHD were not significant for any season ($p>0.05$).

CO_2 differences of ELL and CRAM with MBL were not statistically significant in winter and fall ($p>0.1$). In summer ELL also had similar concentrations as the MBL reference, but CRAM was 7.0 ppm higher (5.6 to 8.5 CI, $p<10^{-15}$). The major differences between ELL and the MBL reference were encountered in spring, being ELL data 2.1 ppm lower on average than MBL (0.7 to 3.6 CI, $p<0.05$). This might indicate that ELL data was more influenced by a regional or continental processes (with strong spring uptake) rather than very local, because the site is usually covered with snow in spring months (Albentosa Sánchez 1973).

4. Discussion

4.1 Annual cycle and growth rate comparison

The comparison of ELL data with other sites showed that ELL mountain station was mostly measuring background concentrations and captured the annual fluctuations driven by global changes. The statistical difference between ELL and the MBL reference was only significant in spring, probably influenced by a

major continental uptake by the former. These results suggest that ELL is a suitable site to help constraining background concentration in European top-down inversion models.

The high mountain sites appeared to have similar behaviors when comparing annual cycles. ELL and CMN annual cycles showed high levels of correlation despite the maximum concentration at ELL was observed in March, a month earlier than at CMN and the MBL reference. In ELL a large decrease of the measured CO_2 concentration was observed in April, probably caused by the influence of the southern Mediterranean vegetation from central Spain that is becoming photosynthetically more active earlier in late winter to early spring (Verger et al. 2016).

The lower summer concentrations observed at CRAM compared to ELL could be explained by higher photosynthesis rates near CRAM station. The surrounding vegetation differs between the two sites, with more mixed and deciduous forests in CRAM compared with meadows, coniferous forests and rocky granite areas in ELL (Figure S1). Winter similitudes are coherent with low average temperatures and the presence of snow at both sites, reducing all kind of CO_2 uptake or release from vegetation or soils (Mast et al. 1998; Merbold et al. 2013). That might also explain the lower differences between ELL and CRAM with the NOAA MBL during winter months.

The strength of the biospheric and oceanic CO_2 exchanges strongly varies in space and time. This variability is, in turn, closely linked back to climatic influences (Goulden 1996; Piao et al. 2013). The annual terrestrial flux indicates the terrestrial CO_2 annual natural budget, i.e. the difference between the natural terrestrial sources and the natural terrestrial sinks (Houghton 2003). The magnitude of the annual growth from the different monitoring sites is correlated with the annual terrestrial flux from MACC-V2 and JENA-MPI biospheric models for the period 2008-2011 (Figure 2). The increase in annual growth in 2010 was coincidental with an increase in the terrestrial flux. Longer time series are however needed to stablish whether this relation is maintained over time.

4.2 Influence of wind direction and atmospheric temperature on CRAM CO_2 concentrations

The amplitude of the CO_2 diurnal cycle at CRAM was highly correlated with temperature following an exponential relation, probably driven by the exponential increase of soil respiration with temperature and the general increase of photosynthesis with temperature at low and mid-temperatures (Berry and Bjorkman 1980; Smith and Dukes 2013). Seasonal changes in boundary layer height caused by temperature annual cycle may also affect the variability of the measured CO_2 (Pino et al. 2013) . The amplitude of the diurnal cycle was also found to be dependent on wind direction. At CRAM annual average temperature (8.1 ºC), the CO_2 diurnal amplitude for days with a predominant wind from N-NW sector was 4.3 ppm lower on average than the diurnal amplitude for days with a predominance of E-SE-S-SW winds. However, the logarithm of the CO_2 diurnal amplitude for both wind sectors co-varied symmetrically with the average daily temperature. A higher CO_2 diurnal signal produced by anthropogenic emissions from vehicles on the N-NW direction, coupled with a similar natural diurnal cycle for both wind sectors, could explain this behavior. Future measurements of CO, which has been widely used as a proxy tracer for fossil fuel-derived CO_2 (Meijer et al. 1996; Vogel et al. 2010; Turnbull et al. 2015) could help determine if the increase in CO_2 concentration from northerly winds was only caused by traffic emissions or was also due to lower vegetation influence.

5. Conclusions

The analysis of the ELL CO_2 series showed that this site behaves as a remote background station that is scarcely influenced by local micrometeorology and local potential sources. The fortnightly samples series are useful to understand the seasonal cycle and the annual growth rate, but poorly serves to know short-term influences. Annual growth rates at ELL were comparable to those observed in remote background locations and correlated with CO_2 terrestrial flux models for 2008-2011.

Continuous data from CRAM showed that CO_2 concentrations were dependent on the wind direction according to the location of local sources and sinks. The near presence of the Vielha tunnel north of the monitoring site influenced the measured concentrations and on average CO_2 concentrations from this direction were ~5 ppm higher on average during daytime. A large amplitude of the CO_2 diurnal cycle (up to 31.4 ppm) was observed in summer. The variability of the diurnal amplitude was proved to be related to the average diurnal temperature due to photosynthesis and soil respiration. The use of a Lloyd and Taylor curve revealed a similar influence of the temperature in the variability of the CO_2 diurnal amplitude for N-NW and

E-SE-S-SW wind sectors. CO_2 traffic emissions could be responsible for an increase of CO_2 concentrations in daytime, lowering the observable amplitude of the CO_2 diurnal cycle when wind was from the N-NW independently of temperature. Future traffic-related tracer measurements such as CO could help resolve the influence of traffic emissions.

The combination of two temporal CO_2 series, one at a high mountain background environment with low time resolution but high precision measurements, and the second in a site more influenced by local emissions, with lower precision but higher time resolution, has been demonstrated to be useful for the study of the sources and sinks controlling the CO_2 budget in mountain ecosystems. Although the precision and accuracy of the GMP343 sensor is low, with a periodic calibration it can improve up to 1.5 ppm. These CO_2 sensors can be useful to study the diurnal variability in remote stations and easy to deploy due to its low maintenance and low energy consumption.

Despite concentrations at the two locations were statistically similar during winter months, summer concentrations showed to be different indicating the presence of more photosynthetic active vegetation near CRAM than at ELL. A future installation of a continuous measurement station near ELL, not directly influenced by anthropogenic emissions, could help resolve the factors driving the diurnal and seasonal CO_2 cycle at ELL. Additional CO_2 flux measurements and soil decomposition studies (tea-bags ILTER global decomposition project, 2016-2019) are already being carried out in grassland areas in the National Park. These measurements will be used to better understand the local influences and the response of ecosystems to temperature changes, and to reduce the uncertainties in the regional carbon balance.

Acknowledgments

The authors would like to acknowledge people from the Aigüestortes i Estany de Sant Maurici National Park, especially Mercè Aniz, for their support on this research. We would also like to thank the University of Barcelona (UB) for their actions and help in installing a continuous measurement station at the Centre de Recerca d'Alta Muntanya (CRAM). We finally thank all the people who participated in the samplings, particularly Helena Parga, Laura Agraz, Rober Sanchez, Cristina Cereza, Montserrat Recolons, Manel Nofuentes, Silvia Borras, Lidia Cañas, Eusebi Vazquez and Paola Occhipinti. We used the Marine Boundary Layer reference product kindly provided by E. Dlugokencky, K. Masarie, P. Lang and P. Tans from NOAA. We used the Obspack CO_2 flask data from Mace Head, CIBA and Monte Cimone stations. We thank all measurement groups for submitting CO_2 concentration data to the Obspack-GLOBALVIEW product. This work has been mainly funded by own resources of the LAO-Climadat Lab at IC3 and by the Fluxpyr project (POCTEFA Program EFA 34/08 - Interreg IV-A). Data is available through virtual access provided and funded in the frame of eLTER H2020 - European Long-Term Ecosystem and Socio-Ecological Research Infrastructure (EC project GA: 654359; INFRAIA; 2015-2019).

References

Albentosa Sánchez LM (1973) Los climas de Catalunya. Estudio de climatología dinámica. Phd Thesis. University of Barcelona

Andrews AE, Kofler JD, Trudeau ME, Williams JC, Neff DH, Masarie KA, Chao DY, Kitzis DR, Novelli PC, Zhao CL, Dlugokencky EJ, Lang PM, Crotwell MJ, Fischer ML, Parker MJ, Lee JT, Baumann DD, Desai AR, Stanier CO, De Wekker SFJ, Wolfe DE, Munger JW, Tans PP (2014) CO2, CO, and CH4 measurements from tall towers in the NOAA earth system research laboratory's global greenhouse gas reference network: Instrumentation, uncertainty analysis, and recommendations for future high-accuracy greenhouse gas monitoring efforts. Atmos Meas Tech 7:647–687 . doi: 10.5194/amt-7-647-2014

Angert A, Biraud S, Bonfils C, Henning CC, Buermann W, Pinzon J, Tucker CJ, Fung I (2005) Drier summers cancel out the CO2 uptake enhancement induced by warmer springs. Proc Natl Acad Sci 102:10823–10827 . doi: 10.1073/pnas.0501647102

Bacardit M, Camarero L (2009) Fluxes of Al, Fe, Ti, Mn, Pb, Cd, Zn, Ni, Cu, and As in monthly bulk deposition over the Pyrenees (SW Europe): The influence of meteorology on the atmospheric component of trace element cycles and its implications for high mountain lakes. J Geophys Res Biogeosciences 114:1–17 . doi: 10.1029/2008JG000732

Bakwin PS, Davis KJ, Yi C, Wofsy SC, Munger JW, Haszpra L, Barcza Z (2004) Regional carbon dioxide fluxes from mixing ratio data. Tellus B 56:301–311 . doi: 10.1111/j.1600-0889.2004.00111.x

Bamberger I, Oney B, Brunner D, Henne S, Leuenberger M, Buchmann N, Eugster W (2017) Observations of

Atmospheric Methane and Carbon Dioxide Mixing Ratios: Tall-Tower or Mountain-Top Stations? Boundary-Layer Meteorol 164:135–159 . doi: 10.1007/s10546-017-0236-3
Bergamaschi P, Krol M, Meirink JF, Dentener F, Segers a., van Aardenne J, Monni S, Vermeulen AT, Schmidt M, Ramonet M, Yver C, Meinhardt F, Nisbet EG, Fisher RE, O'Doherty S, Dlugokencky EJ (2010) Inverse modeling of European CH4 emissions 2001–2006. J Geophys Res 115:D22309 . doi: 10.1029/2010JD014180
Berry J, Bjorkman O (1980) Photosynthetic Response and Adaptation to Temperature in Higher Plants. Annu Rev Plant Physiol 31:491–543 . doi: 10.1146/annurev.pp.31.060180.002423
Bouwman AF (1989) The role of soils and land use in the greenhouse effect. Netherlands J. Agric. Sci. 37:13–19
Bowman AW, Azzalini A (1997) Applied Smoothing Techniques for Data Analysis: the Kernel Approach with S-Plus Illustrations. Oxford University Press, Oxford
Camarero L, Bacardit M, de Diego A, Arana G (2017) Decadal trends in atmospheric deposition in a high elevation station: Effects of climate and pollution on the long-range flux of metals and trace elements over SW Europe. Atmos Environ 167:542–552 . doi: 10.1016/j.atmosenv.2017.08.049
Camarero L, Catalan J (1993) Chemistry of bulk precipitation in the central and eastern Pyrenees, northeast Spain. Atmos Environ Part A, Gen Top 27:83–94 . doi: 10.1016/0960-1686(93)90073-8
Camarero L, Catalan J, Morgui JA, Gacia E (2018) Daily meteorology (wind, air temperature, humidity, precipitation, radiation) from 2005-2017 for Aigüestortes LTER site. https://b2share.eudat.eu/records/3e0968efd0994389b2ce59f0bca3adc5. Accessed 20 Jun 2018
Camarero L, Morguí J-A (2009) Recerca ecològica a llarg termini en el Parc Nacional: el node LTER-Aigüestortes. In: Actas de las VIII Jornadas sobre Investigación del Parque Nacional de Aigüestortes i Estany de Sant Maurici. Espot, (Lleida). Departament de Medi Ambient i Habitatge, Generalitat de Catalunya. Barcelona. España.
Carreras J, Diego F (2007) Cartografia dels hàbitats a Catalunya 1: 50.000. In: General. Catalunya
Carrillo E, Ninot JM (1992) Flora i vegetació de les valls d'Espot i Boí. Arx. la secció Ciències l'Institut d'Estudis Catalans 99:474 + 350
Carslaw DC, Ropkins K (2012) openair — An R package for air quality data analysis. Environ Model Softw 27–28:52–61 . doi: 10.1016/j.envsoft.2011.09.008
Catalan J (1989) The winter cover of a high-mountain Mediterranean lake (Estany Redó, Pyrenees). Water Resour Res 25:519–527 . doi: 10.1029/WR025i003p00519
Chappuis E, Gacia E, Ballesteros E (2011) Changes in aquatic macrophyte flora over the last century in Catalan water bodies (NE Spain). Aquat Bot 95:268–277 . doi: 10.1016/j.aquabot.2011.08.006
Chappuis E, Gacia E, Ballesteros E (2014) Environmental factors explaining the distribution and diversity of vascular aquatic macrophytes in a highly heterogeneous Mediterranean region. Aquat Bot 113:72–82 . doi: 10.1016/j.aquabot.2013.11.007
Chevallier F, Ciais P, Conway TJ, Aalto T, Anderson BE, Bousquet P, Brunke EG, Ciattaglia L, Esaki Y, Fröhlich M, Gomez A, Gomez-Pelaez AJ, Haszpra L, Krummel PB, Langenfelds RL, Leuenberger M, MacHida T, Maignan F, Matsueda H, Morguí JA, Mukai H, Nakazawa T, Peylin P, Ramonet M, Rivier L, Sawa Y, Schmidt M, Steele LP, Vay SA, Vermeulen AT, Wofsy S, Worthy D (2010) CO2 surface fluxes at grid point scale estimated from a global 21 year reanalysis of atmospheric measurements. J Geophys Res Atmos 115:1–17 . doi: 10.1029/2010JD013887
Ciais P, Peylin P, Bousquet P (2000) Regional Biospheric Carbon Fluxes as Inferred from Atmospheric CO2 Measurements. Ecol Appl 10:1574 . doi: 10.2307/2641225
Ciais P, Rayner P, Chevallier F, Bousquet P, Logan M, Peylin P, Ramonet M (2010) Atmospheric inversions for estimating CO2 fluxes: Methods and perspectives. Clim Change 103:69–92 . doi: 10.1007/s10584-010-9909-3
Ciattaglia L (1983) Interpretation of atmospheric CO2 measurements at Mt. Cimone (Italy) related to wind data. J Geophys Res 88:1331 . doi: 10.1029/JC088iC02p01331
Ciattaglia L, Cundari V, Colombo T (1987) Further measurements of atmospheric carbon dioxide at Mt. Cimone, Italy: 1979–1985. Tellus B 39 B:13–20 . doi: 10.1111/j.1600-0889.1987.tb00266.x
Colombo T, Santaguida R, Capasso A, Calzolari F, Evangelisti F, Bonasoni P (2000) Biospheric influence on carbon dioxide measurements in Italy. Atmos Environ 34:4963–4969 . doi: 10.1016/S1352-2310(00)00366-6
Conway TJ, Tans PP, Waterman LS, Thoning KW, Kitzis DR, Masarie KA, Zhang N (1994) Evidence for interannual variability of the carbon cycle from the National Oceanic and Atmospheric Administration Climate Monitoring and Diagnostics Laboratory Global Air Sampling Network. J Geophys Res - Atmos 99:22831–22855 . doi: 10.1029/94JD01951
Cooperative Global Atmospheric Data Integration Project; (2017): Multi-laboratory compilation of atmospheric carbon dioxide data for the period 1957-2016 (2017) obspack_co2_1_GLOBALVIEWplus_v3.2_2017_11_02; NOAA Earth System Research Laboratory,

Global Monitoring Division. http://dx.doi.org/10.15138/G3704H. Accessed 1 Oct 2018
Cooperative Global Atmospheric Data Integration Project. 2013 updated annually. M compilation of synchronized and gap-filled atmospheric carbon dioxide records for the period 1979-2012 (2013) obspack_co2_1_GLOBALVIEW-CO2_2013_v1.0.4_2013-12-23 . Compiled by NOAA Global Monitoring Division: Boulder, Colorado, U.S.A. http://dx.doi.org/10.3334/OBSPACK/1002. Accessed 1 Oct 2018
Cristofanelli P, Brattich E, Decesari S, Landi TC, Maione M, Putero D, Tositti L, Bonasoni P (2018) The "O. Vittori" Observatory at Mt. Cimone: A "Lighthouse" for the Mediterranean Troposphere. High-Mountain Atmos Res SpringerBriefs Meteorol Springer, Cham. doi: 10.1007/978-3-319-61127-3_1
Crosson ER (2008) A cavity ring-down analyzer for measuring atmospheric levels of methane, carbon dioxide, and water vapor. Appl Phys B Lasers Opt 92:403–408 . doi: 10.1007/s00340-008-3135-y
Cundari V, Colombo T, Ciattaglia L (1995) Thirteen years of atmospheric carbon dioxide measurements at Mt. Cimone station, Italy. Nuovo Cim C 18:33–47 . doi: 10.1007/BF02561457
Cundari V, Colombo T, Papini G, Benedicti G, Ciattaglia L (1990) Recent improvements on atmospheric CO2 measurements at Mt. Cimone observatory, Italy. Nuovo Cim C 13:871–882 . doi: 10.1007/BF02512003
Curcoll R, Recolons M, Font A, Agraz L, Parga E, Bacardit E, Camarero L, Pueyo S, Rodó X, Morguí JA (2010) First 2 years of Atmospheric CO2 measurements in the Estany Llong plain (2100 masl, Parc Nacional d'Aigüestortes i Estany de Sant Maurici, Pyrenees, Catalonia, Spain). In: EGU General Assembly Conference Abstracts. p 3608
Dlugokencky EJ, Lang PM, Mund JW, Crotwell AM, Crotwell MJ, Thoning KW (2017a) Atmospheric Carbon Dioxide Dry Air Mole Fractions from the NOAA ESRL Carbon Cycle Cooperative Global Air Sampling Network.1968-2016, Version: 2017-07-28. ftp://aftp.cmdl.noaa.gov/data/trace_gases/co2/flask/surface/. Accessed 1 Oct 2018
Dlugokencky EJ, Thoning KW, Lang PM, Tans PP (2017b) NOAA Greenhouse Gas Reference from Atmospheric Carbon Dioxide Dry Air Mole Fractions from the NOAA ESRL Carbon Cycle Cooperative Global Air Sampling Network. ftp://aftp.cmdl.noaa.gov/data/trace_gases/co2/flask/surface/. Accessed 1 Oct 2018
Geels C, Gloor M, Ciais P, Bousquet P, Peylin P, Vermeulen a. T, Dargaville R, Aalto T, Brandt J, Christensen JH, Frohn LM, Haszpra L, Karstens U, Rödenbeck C, Ramonet M, Carboni G, Santaguida R (2007) Comparing atmospheric transport models for future regional inversions over Europe - Part 1: mapping the atmospheric CO2 signals. Atmos Chem Phys 7:3461–3479 . doi: 10.5194/acp-7-3461-2007
Gomez-Pelaez AJ, Ramos R (2011) Improvements in the Carbon Dioxide and Methane Continuous Measurement Programs at Izaña Global GAW Station (Spain) during 2007-2009. In: Rep. 15th WMO/IAEA Meet. Expert. Carbon Diox ide, Other Greenh. Gases, Relat. Tracer Meas. Tech. 7–10 Sept. 2009, GAW Rep. number 194, WMO TD 1553. https://library.wmo.int/pmb_ged/wmo-td_1553.pdf. Accessed 1 Oct 2018
Goulden ML (1996) Exchange of carbon dioxide by a deciduous forest: Response to interannual climate variability. Science (80-) 271:1576–1578 . doi: 10.1126/science.271.5255.1576
Hase F, Frey M, Blumenstock T, Groß J, Kiel M, Kohlhepp R, Mengistu Tsidu G, Schäfer K, Sha MK, Orphal J (2015) Application of portable FTIR spectrometers for detecting greenhouse gas emissions of the major city Berlin. Atmos Meas Tech 8:3059–3068 . doi: 10.5194/amt-8-3059-2015
Hervàs A, Camarero L, Reche I, Casamayor EO (2009) Viability and potential for immigration of airborne bacteria from Africa that reach high mountain lakes in Europe. Environ Microbiol 11:1612–1623 . doi: 10.1111/j.1462-2920.2009.01926.x
Houghton RA (2003) Revised estimates of the annual net flux of carbon to the atmosphere from changes in land use and land management 1850-2000. Tellus, Ser B Chem Phys Meteorol 55:378–390 . doi: 10.1034/j.1600-0889.2003.01450.x
Hu C, Griffis TJ, Lee X, Millet DB, Chen Z, Baker JM, Xiao K (2018) Top-Down Constraints on Anthropogenic CO2 Emissions Within an Agricultural-Urban Landscape. J Geophys Res Atmos 123:4674–4694 . doi: 10.1029/2017JD027881
Le Quéré C, Andrew RM, Canadell JG, Sitch S, Korsbakken JI, Peters GP, Manning AC, Boden TA, Tans PP, Houghton RA, Keeling RF, Alin S, Andrews OD, Anthoni P, Barbero L, Bopp L, Chevallier F, Chini LP, Ciais P, Currie K, Delire C, Doney SC, Friedlingstein P, Gkritzalis T, Harris I, Hauck J, Haverd V, Hoppema M, Klein Goldewijk K, Jain AK, Kato E, Körtzinger A, Landschützer P, Lefèvre N, Lenton A, Lienert S, Lombardozzi D, Melton JR, Metzl N, Millero F, Monteiro PMSS, Munro DR, Nabel JEMSMS, Nakaoka SI, O'Brien K, Olsen A, Omar AM, Ono T, Pierrot D, Poulter B, Rödenbeck C, Salisbury J, Schuster U, Schwinger J, Séférian R, Skjelvan I, Stocker BD, Sutton AJ, Takahashi T, Tian H, Tilbrook B, van der Laan-Luijkx IT, van der Werf GR, Viovy N, Walker AP, Wiltshire AJ, Zaehle S, Ivar Korsbakken J, Peters GP, Manning AC, Boden TA, Tans PP, Houghton RA, Keeling RF, Alin S, Andrews OD, Anthoni P, Barbero L, Bopp L, Chevallier F, Chini LP, Ciais P, Currie K, Delire C, Doney SC, Friedlingstein P, Gkritzalis T, Harris I, Hauck J, Haverd V, Hoppema M, Klein Goldewijk K, Jain AK, Kato E, Körtzinger A, Landschützer P, Lefèvre N, Lenton A, Lienert S, Lombardozzi D, Melton JR, Metzl N, Millero F,

Monteiro PMSS, Munro DR, Nabel JEMSMS, Nakaoka SI, O'Brien K, Olsen A, Omar AM, Ono T, Pierrot D, Poulter B, Rödenbeck C, Salisbury J, Schuster U, Schwinger J, Séférian R, Skjelvan I, Stocker BD, Sutton AJ, Takahashi T, Tian H, Tilbrook B, van der Laan-Luijkx IT, van der Werf GR, Viovy N, Walker AP, Wiltshire AJ, Zaehle S (2016) Global Carbon Budget 2016. Earth Syst Sci Data 8:605–649 . doi: 10.5194/essd-8-605-2016

Levin I (1987) Atmospheric CO2 in continental European alternative approach to clean air CO2 data. Tellus 39B:21–28 . doi: 10.1111/j.1600-0889.1987.tb00267.x

Lloyd J, Taylor J (1994) On the temperature dependence of soil respiration. Funct Ecol 8:315–323 . doi: 10.2307/2389824

Marquis M, Tans P (2008) CLIMATE CHANGE: Carbon Crucible. Science (80-) 320:460–461 . doi: 10.1126/science.1156451

Masarie KA, Tans PP (1995) Extension and integration of atmospheric carbon dioxide data into a globally consistent measurement record. J Geophys Res 100:11593 . doi: 10.1029/95JD00859

Mast MA, Wickl KP, Striegl RT, W. Clow D (1998) Winter fluxes of CO2 and CH4 from subalpine soils in Rocky Mountain National Park, Colorado. Global Biogeochem Cycles 12:607–620 . doi: 10.1029/98GB02313

Meijer HAJ, Smid HM, Perez E, Keizer MG (1996) Isotopic characterisation of anthropogenic CO2 emissions using isotopic and radiocarbon analysis. Phys Chem Earth 21:483–487 . doi: 10.1016/S0079-1946(97)81146-9

Merbold L, Steinlin C, Hagedorn F (2013) Winter greenhouse gas fluxes (CO2, CH4 and N2O) from a subalpine grassland. Biogeosciences 10:3185–3203 . doi: 10.5194/bg-10-3185-2013

Ninyerola M, Pons X, Roure JM, Martin VJ, Raso J, Clavero P (2003) Atles climàtic digital de Catalunya. In: Serv. Meteorològic Catalunya i Dep. Medi Ambient General. Catalunya Barcelona. http://www.opengis.uab.cat/acdc/en_index.htm. Accessed 1 Oct 2018

Peylin P, Law RM, Gurney KR, Chevallier F, Jacobson AR, Maki T, Niwa Y, Patra PK, Peters W, Rayner PJ, Rödenbeck C, Van Der Laan-Luijkx IT, Zhang X (2013) Global atmospheric carbon budget: Results from an ensemble of atmospheric CO2 inversions. Biogeosciences 10:6699–6720 . doi: 10.5194/bg-10-6699-2013

Piao S, Sitch S, Ciais P, Friedlingstein P, Peylin P, Wang X, Ahlström A, Anav A, Canadell JG, Cong N, Huntingford C, Jung M, Levis S, Levy PE, Li J, Lin X, Lomas MR, Lu M, Luo Y, Ma Y, Myneni RB, Poulter B, Sun Z, Wang T, Viovy N, Zaehle S, Zeng N (2013) Evaluation of terrestrial carbon cycle models for their response to climate variability and to CO2 trends. Glob Chang Biol 19:2117–2132 . doi: 10.1111/gcb.12187

Pickers PA, Manning AC (2015) Investigating bias in the application of curve fitting programs to atmospheric time series. Atmos Meas Tech 8:1469–1489 . doi: 10.5194/amt-8-1469-2015

Pillai D, Gerbig C, Ahmadov R, Rödenbeck C, Kretschmer R, Koch T, Thompson R, Neininger B, Lavrié J V. (2011) High-resolution simulations of atmospheric CO2 over complex terrain-representing the Ochsenkopf mountain tall tower. Atmos Chem Phys 11:7445–7464 . doi: 10.5194/acp-11-7445-2011

Pino D, Kaikkonen J-P, de Arellano JV-G (2013) Quantifying the uncertainties of advection and boundary layer dynamics on the diurnal carbon dioxide budget. J Geophys Res Atmos 118:9376–9392 . doi: 10.1002/jgrd.50677

Post WM, Peng T-HH, Emanuel WR, King AW, Dale VH, DeAngelis DL (1990) The Global Carbon Cycle. Am Sci 78:892–895

Potter CSC, Randerson J (1993) Terrestrial ecosystem production: a process model based on global satellite and surface data. Global Biogeochem Cycles 7:811–841 . doi: 10.1029/93GB02725

Pumpanen J, Ilvesniemi H, Kulmala L, Siivola E, Laakso H, Kolari P, Helenelund C, Laakso M, Uusimaa M, Hari P (2008) Respiration in Boreal Forest Soil as Determined from Carbon Dioxide Concentration Profile. Soil Sci Soc Am J 72:1187 . doi: 10.2136/sssaj2007.0199

Randerson JT, Field CB, Fung IY, Tans PP (1999) Increases in early season ecosystem uptake explain recent changes in the seasonal cycle of atmospheric CO2 at high northern latitudes. Geophys Res Lett 26:2765–2768 . doi: 10.1029/1999GL900500

Reichstein M, Falge E, Baldocchi D, Papale D, Aubinet M, Berbigier P, Bernhofer C, Buchmann N, Gilmanov T, Granier A, Grunwald T, Havrankova K, Ilvesniemi H, Janous D, Knohl A, Laurila T, Lohila A, Loustau D, Matteucci G, Meyers T, Miglietta F, Ourcival J-M, Pumpanen J, Rambal S, Rotenberg E, Sanz M, Tenhunen J, Seufert G, Vaccari F, Vesala T, Yakir D, Valentini R (2005) On the separation of net ecosystem exchange into assimilation and ecosystem respiration: review and improved algorithm. Glob Chang Biol 11:1424–1439 . doi: 10.1111/j.1365-2486.2005.001002.x

Rella CW, Chen H, Andrews AE, Filges A, Gerbig C, Hatakka J, Karion A, Miles NL, Richardson SJ, Steinbacher M, Sweeney C, Wastine B, Zellweger C (2013) High accuracy measurements of dry mole fractions of carbon dioxide and methane in humid air. Atmos Meas Tech 6:837–860 . doi: 10.5194/amt-6-

837-2013
Richardson SJ, Miles NL, Davis KJ, Crosson ER, Rella CW, Andrews AE (2012) Field testing of cavity ring-down spectroscopy analyzers measuring carbon dioxide and water vapor. J Atmos Ocean Technol 29:397–406 . doi: 10.1175/JTECH-D-11-00063.1
Rigby M, Toumi R, Fisher R, Lowry D, Nisbet EG (2008) First continuous measurements of CO2 mixing ratio in central London using a compact diffusion probe. Atmos Environ 42:8943–8953 . doi: 10.1016/j.atmosenv.2008.06.040
Rödenbeck C, Houweling S, Gloor M, Heimann M (2003) CO2 flux history 1982–2001 inferred from atmospheric data using a global inversion of atmospheric transport. Atmos Chem Phys 3:1919–1964 . doi: 10.5194/acp-3-1919-2003
Sánchez ML, Pérez IA, García MA (2010) Study of CO2 variability at different temporal scales recorded in a rural Spanish site. Agric For Meteorol 150:1168–1173 . doi: 10.1016/j.agrformet.2010.04.018
Schibig MF, Steinbacher M, Buchmann B, Van Der Laan-Luijkx IT, Van Der Laan S, Ranjan S, Leuenberger MC (2015) Comparison of continuous in situ CO2 observations at Jungfraujoch using two different measurement techniques. Atmos Meas Tech 8:57–68 . doi: 10.5194/amt-8-57-2015
Schmidt M (2003) The Schauinsland CO2 record: 30 years of continental observations and their implications for the variability of the European CO2 budget. J Geophys Res 108:4619 . doi: 10.1029/2002JD003085
Smith NG, Dukes JS (2013) Plant respiration and photosynthesis in global-scale models: Incorporating acclimation to temperature and CO2. Glob Chang Biol 19:45–63 . doi: 10.1111/j.1365-2486.2012.02797.x
Sturm P, Leuenberger M, Sirignano C, Neubert REM, Meijer HAJ, Langenfelds R, Brand WA, Tohjima Y (2004) Permeation of atmospheric gases through polymer O-rings used in flasks for air sampling. J Geophys Res Atmos 109:n/a-n/a . doi: 10.1029/2003JD004073
Tans PP, Fung IY, Takahashi T (1990a) Observational Constraints on the Global Atmospheric CO2 Budget. Science (80-) 247:1431–1438 . doi: 10.1126/science.247.4949.1431
Tans PP, Thoning KW, Elliott WP, Conway TJ (1990b) Error estimates of background atmospheric CO2 patterns from weekly flask samples. J Geophys Res 95:14063 . doi: 10.1029/JD095iD09p14063
Thoning KW, Tans PP, Komhyr WD (1989) Atmospheric carbon dioxide at Mauna Loa Observatory: 2. Analysis of the NOAA GMCC data, 1974-1985. J Geophys Res Atmos 94:8549–8565 . doi: 10.1029/JD094iD06p08549
Turnbull JC, Sweeney C, Karion A, Newberger T, Lehman SJ, Tans PP, Davis KJ, Lauvaux T, Miles NL, Richardson SJ, Cambaliza MO, Shepson PB, Gurney K, Patarasuk R, Razlivanov I (2015) Toward quantification and source sector identification of fossil fuel CO2 emissions from an urban area: Results from the INFLUX experiment. J Geophys Res Atmos 120:292–312 . doi: 10.1002/2014JD022555
Vaisala (2017) Vaisala CARBOCAP Carbon Dioxide Probe GMP343. In: Vaisala Oyj, Finl. https://www.vaisala.com/sites/default/files/documents/GMP343-Datasheet-B210688EN-F.pdf. Accessed 1 Oct 2018
Verger A, Filella I, Baret F, Peñuelas J (2016) Vegetation baseline phenology from kilometric global LAI satellite products. Remote Sens Environ 178:1–14 . doi: 10.1016/j.rse.2016.02.057
Vogel FR, Hammer S, Steinhof A, Kromer B, Levin I (2010) Implication of weekly and diurnal 14C calibration on hourly estimates of CO-based fossil fuel CO2 at a moderately polluted site in southwestern Germany. Tellus, Ser B Chem Phys Meteorol 62:512–520 . doi: 10.1111/j.1600-0889.2010.00477.x
Young SG, Bowman AW (1995) Non-Parametric Analysis of Covariance. Biometrics 51:920–931 . doi: 10.2307/2532993
Zhao CL, Tans PP (2006) Estimating uncertainty of the WMO mole fraction scale for carbon dioxide in air. J Geophys Res 111:D08S09 . doi: 10.1029/2005JD006003

Table1. Parameters of the Lloyd and Taylor curve depending on forthcoming wind direction.

Forthcoming wind direction	A	E_0	R^2
N-NW	2469	282.6	0.65
E-SE-S-SW	3699	289.5	0.72

FIGURE CAPTIONS

Figure 1. Observed CO_2 time series from 2008-2014 based on Estany Llong (ELL) fortnightly CO_2 data series (red points), ELL CO_2 4–harmonics fit (straight line), NOAA Marine Boundary Layer (MBL) reference (dashed line) and the Centre de Recerca d'Alta Muntanya (CRAM) hourly CO_2 data series (green small dots).

Figure 2: Observed CO_2 annual growth rate of Estany Llong (ELL), NOAA Marine Boundary Layer (MBL) reference, Mace Head (MHD), CIBA (CIB) and Monte Cimone (CMN) data series. Annual global CO_2 terrestrial flux as MACC V2 and JENA MPI models are shown for years 2008-2011 on the right axis. Vertical lines are the standard deviations of annual growth rates.

Figure 3: a) Wind rose for flask sampling events at Estany Llong (ELL) b) Polar plot of CO_2 residuals from the 4-harmonics fit curve at ELL. WSpeed: wind speed (m/s)

Figure 4: Influence of wind direction on the observed CO_2 data measured at Centre de Recerca d'Alta Muntanya (CRAM). Bivariate polar plots of CO_2 data: a) Average 2010-2014; b) Diurnal (08 to 20 GMT); c) Nocturnal (22 to 05 GMT); d) Summer (May to October); e) Winter (November to April). WSpeed: wind speed (m/s)

Figure 5: Influence of temperature on the observed CO_2 data measured at Centre de Recerca d'Alta Muntanya (CRAM). Natural logarithm of CO_2 diurnal amplitude against daily mean temperature for N-NW coming winds and for E-SE-S-SW winds and their corresponding Lloyd & Taylor fit (Lloyd and Taylor 1994).

Figure 6: Average annual CO_2 cycle measured from the observed data at Centre de Recerca d'Alta Muntanya (CRAM), Estany Llong (ELL), Mace Head (MHD), Monte Cimone (CMN), CIBA (CIB) and NOAA Marine Boundary Layer (MBL) reference for the period 2010-2013. Shaded regions are the interquartile ranges for CRAM (light red) and ELL (grey).

SUPPLEMENTARY MATERIAL

Figure S1. General location of Aigüestortes Long Term Ecological Research site in the Pyrenees chain (left). Location of Centre de Recerca d'Alta Muntanya (CRAM) and Estany Llong (ELL) stations in the park (top-center). Corine land cover maps from the cartography of habitats in Catalonia (Carreras and Diego 2007) around CRAM (top left) and ELL (bottom left).

Figure S2: Schematic for the CO_2 analysis of flask samples using two Licor7000 analyzers.

Figure S3: Diurnal and annual CO_2 variability at Centre de Recerca d'Alta Muntanya (CRAM). Trend level plot for CO_2 at CRAM for 2010, 2011, 2012 and 2013.

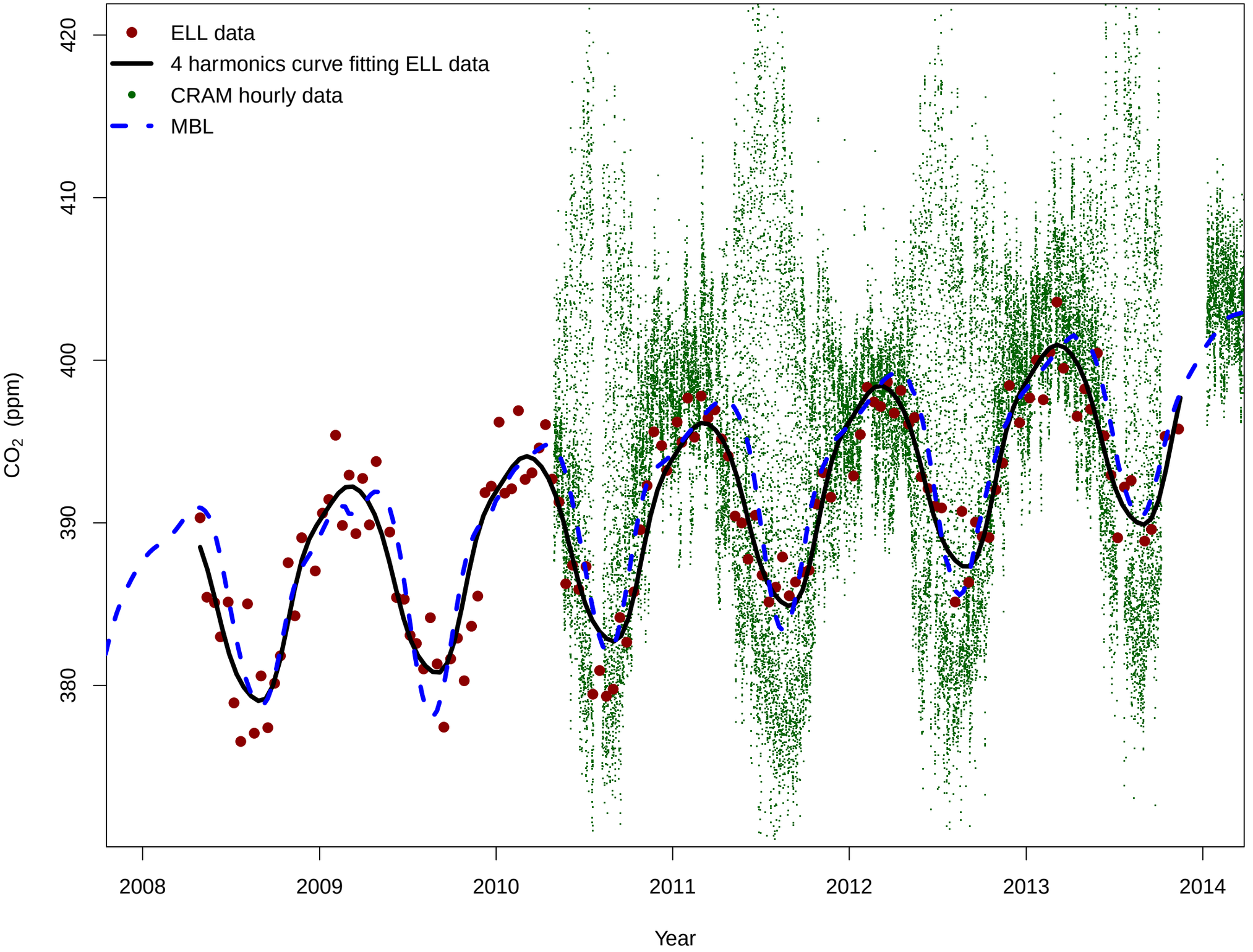
ELL data
4 harmonics curve fitting ELL data
CRAM hourly data
MBL
420
410
400
390
380
CO2 (ppm)
2008
2009
2010
2011
2012
2013
2014
Year

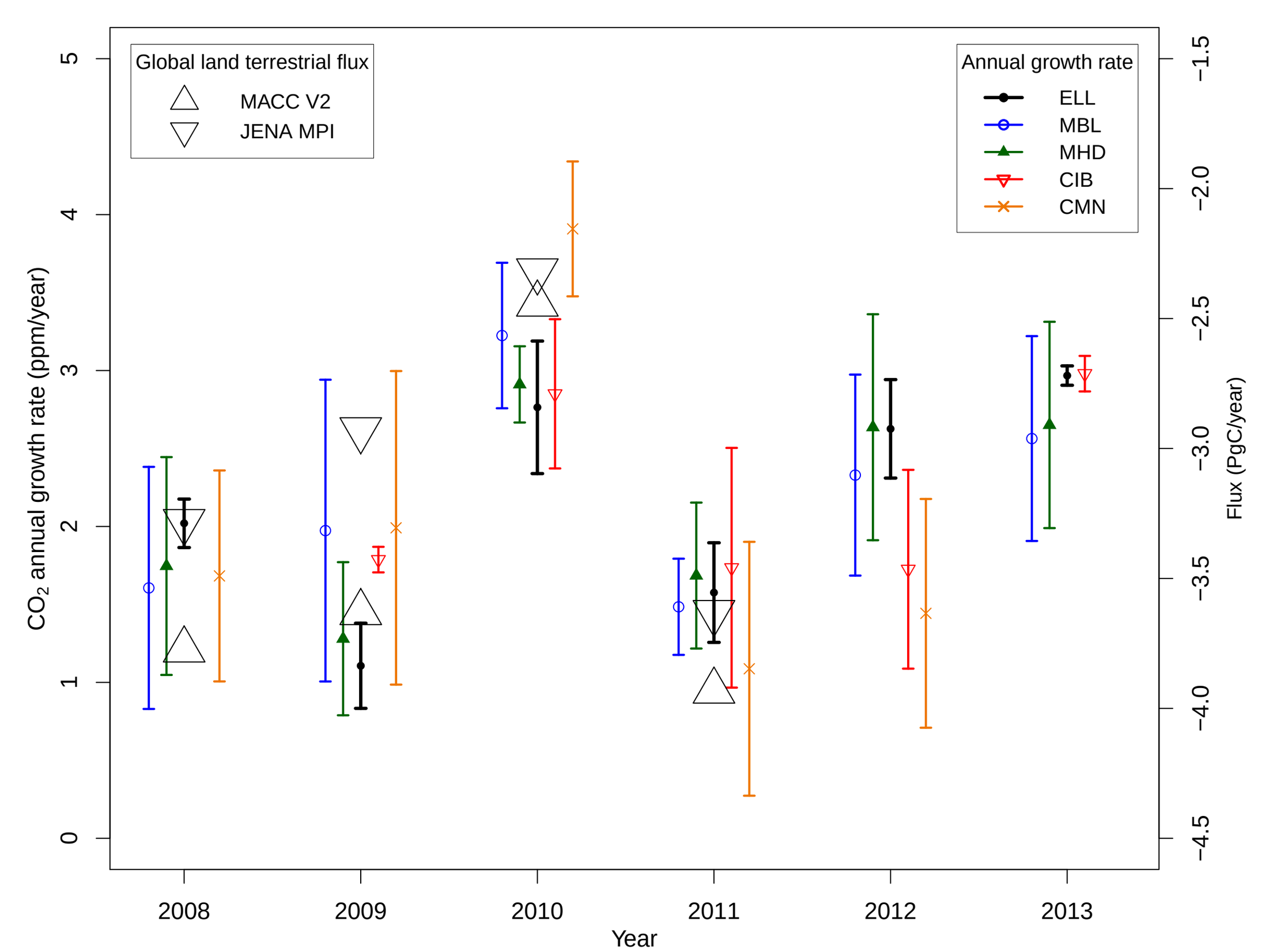
Global land terrestrial flux
MACC V2
JENA MPI
Annual growth rate
ELL
MBL
MHD
CIB
CMN
CO2 annual growth rate (ppm/year)
Flux (PgC/year)
Year
2008
2009
2010
2011
2012
2013
0
1
2
3
4
5
−1.5
−2.0
−2.5
−3.0
−3.5
−4.0
−4.5

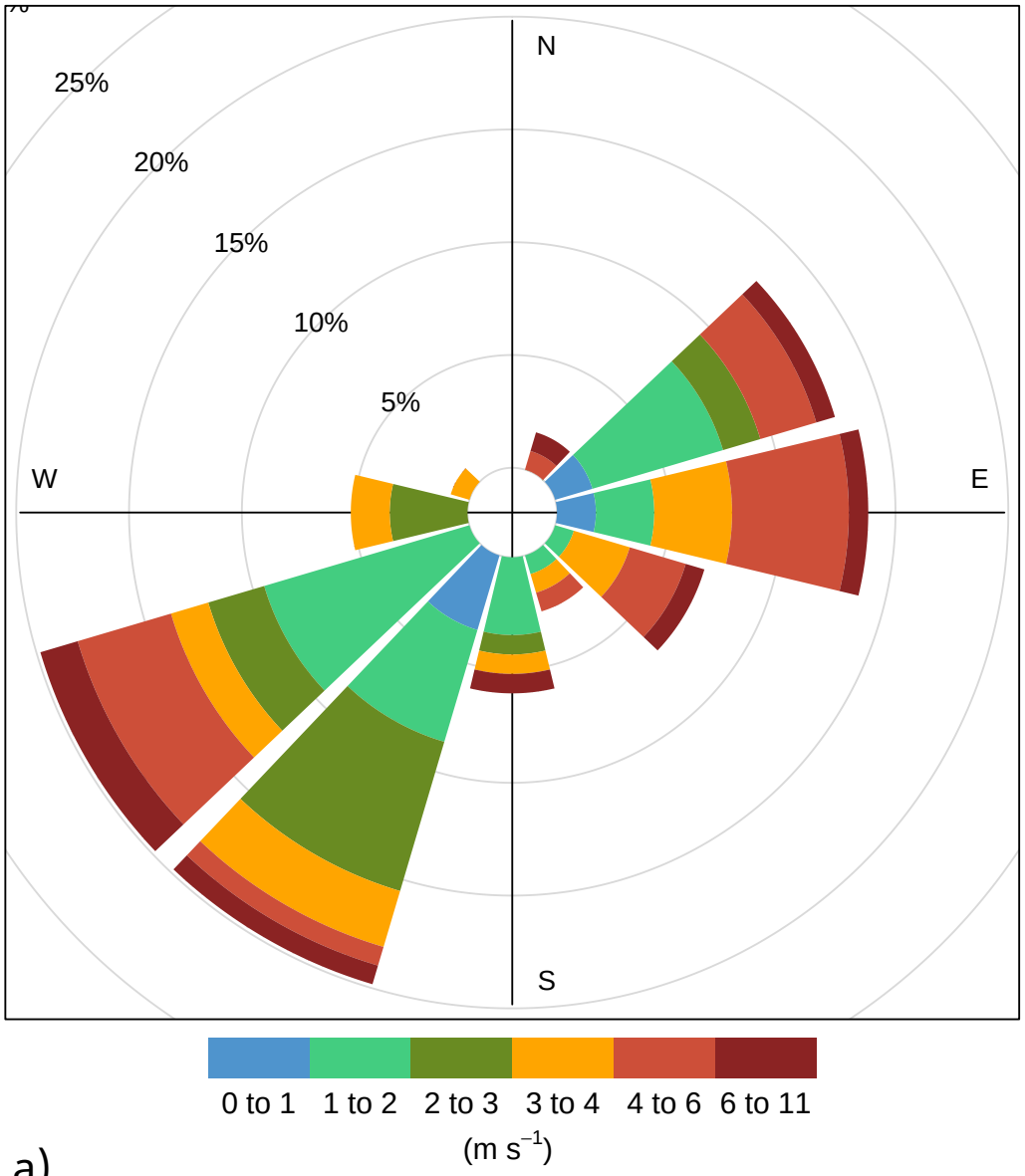
N
E
S
W
25%
20%
15%
10%
5%
0 to 1
1 to 2
2 to 3
3 to 4
4 to 6
6 to 11
(m s⁻¹)

a)

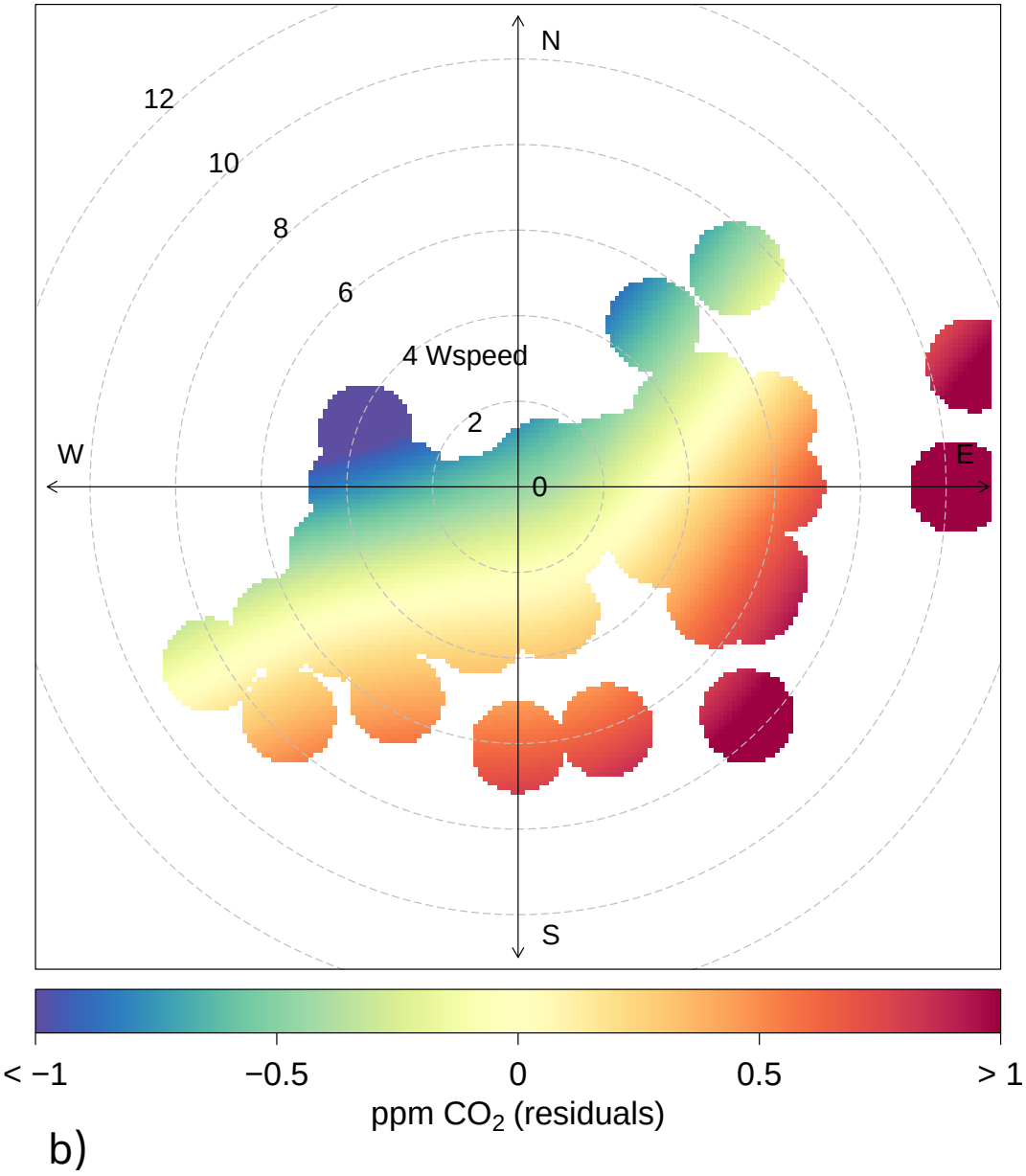
N
E
S
W
12
10
8
6
4 Wspeed
2
0
< −1
−0.5
0
0.5
> 1
ppm CO2 (residuals)

b)

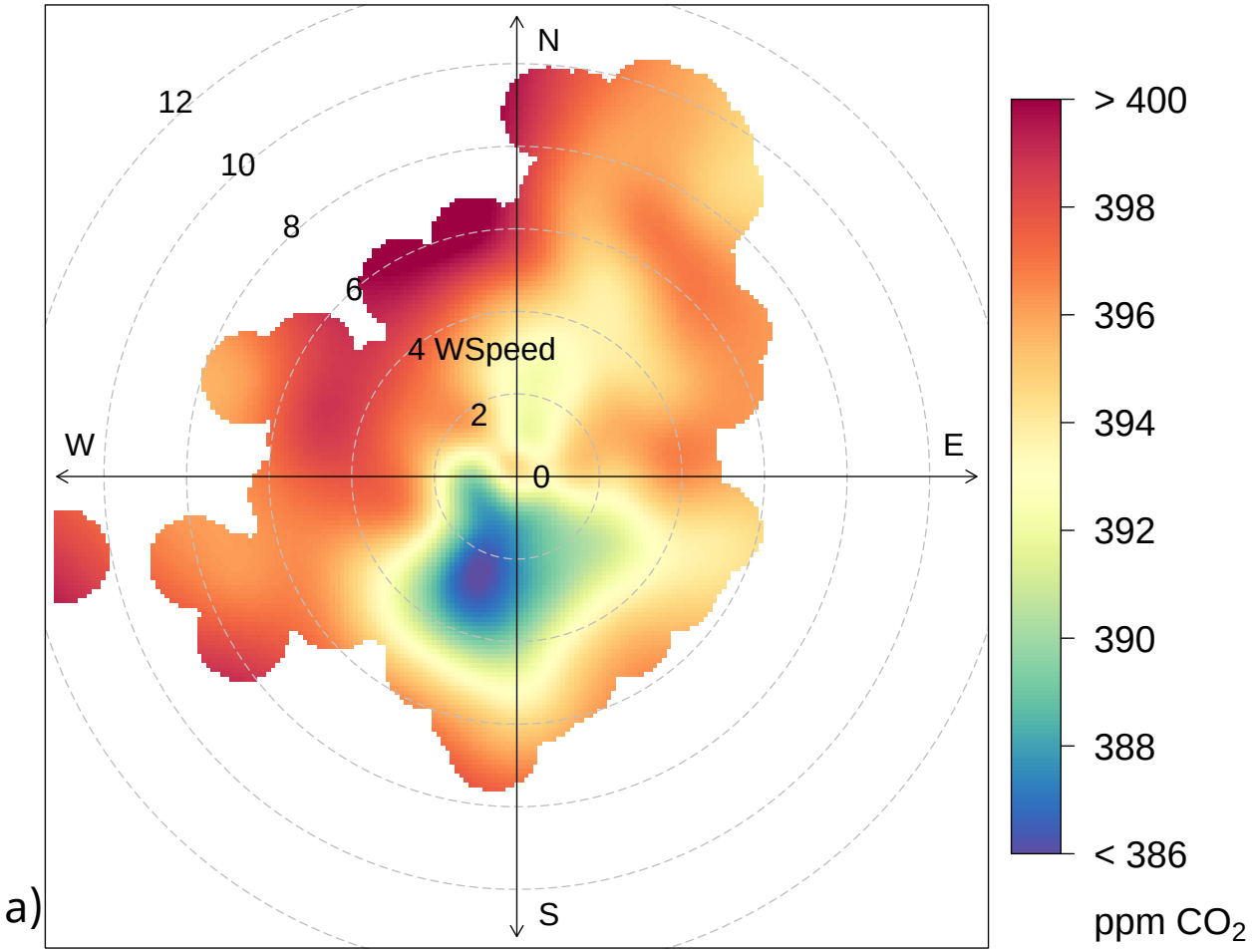
N
S
W
E
12
10
8
6
4 WSpeed
2
0
a)
> 400
398
396
394
392
390
388
< 386
ppm CO_2
b)
c)
d)
e)

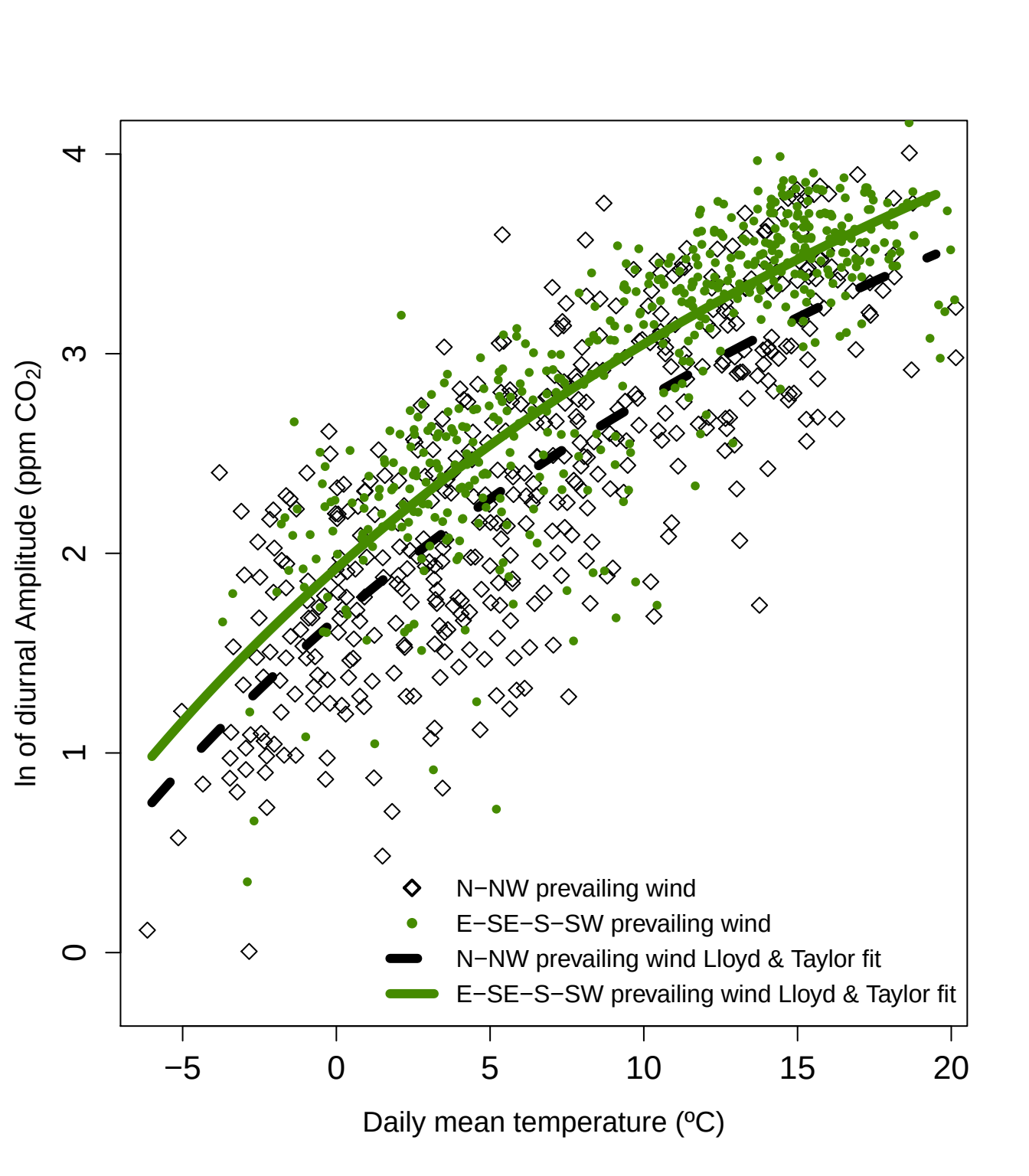
ln of diurnal Amplitude (ppm CO_2)
0
1
2
3
4
−5
0
5
10
15
20
Daily mean temperature (ºC)
N−NW prevailing wind
E−SE−S−SW prevailing wind
N−NW prevailing wind Lloyd & Taylor fit
E−SE−S−SW prevailing wind Lloyd & Taylor fit

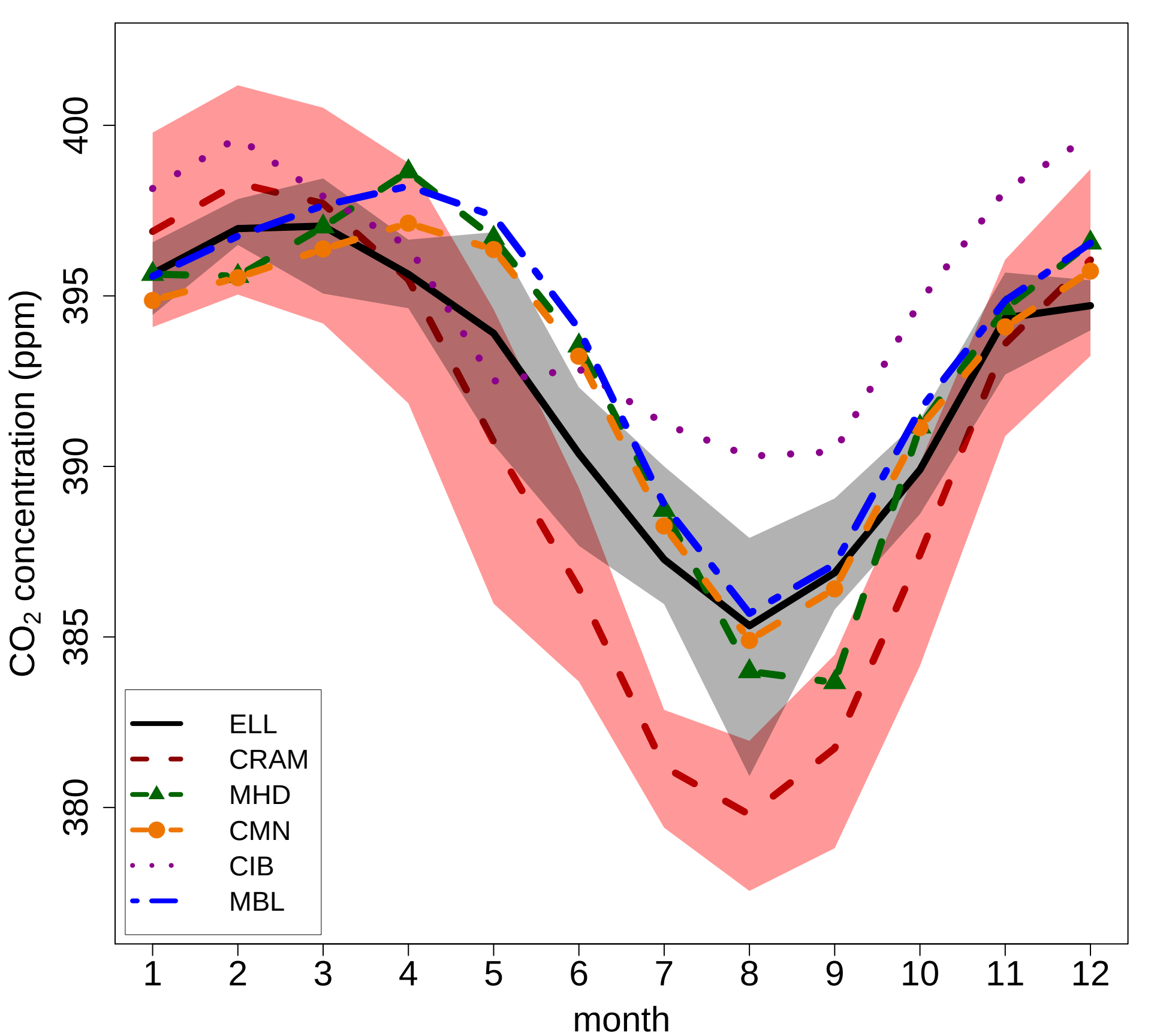
400
395
390
385
380
CO_2 concentration (ppm)
1
2
3
4
5
6
7
8
9
10
11
12
month
ELL
CRAM
MHD
CMN
CIB
MBL

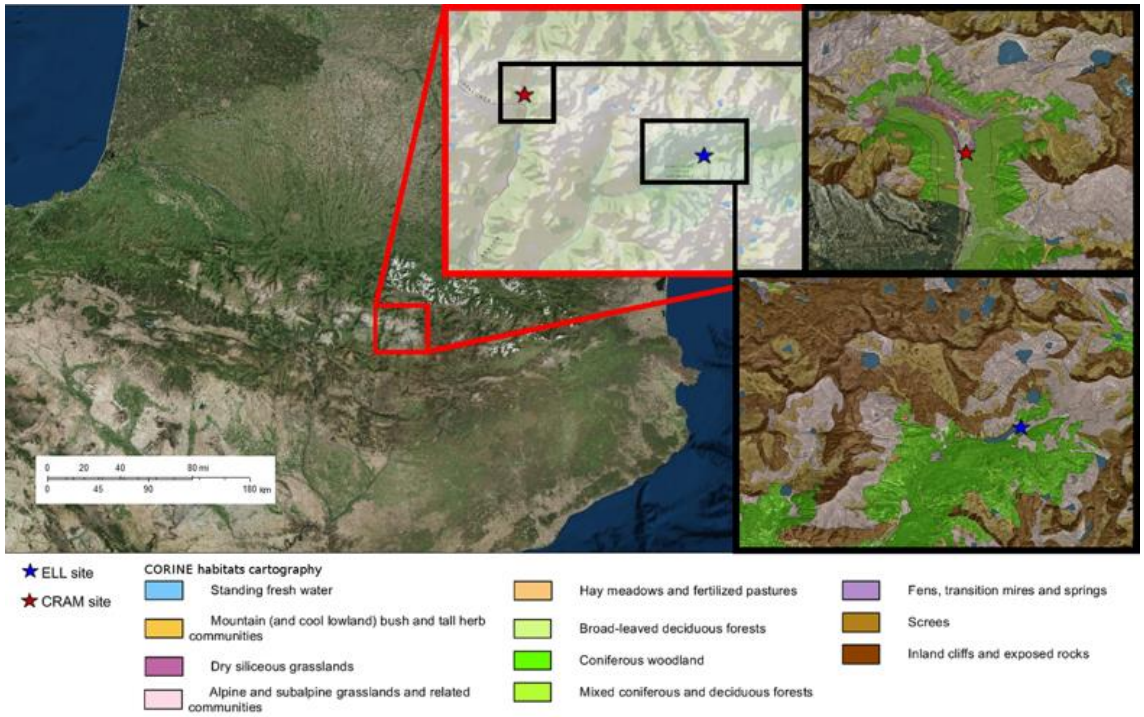
0 20 40 80 mi
0 45 90 180 km
ELL site
CRAM site
CORINE habitats cartography
Standing fresh water
Mountain (and cool lowland) bush and tall herb communities
Dry siliceous grasslands
Alpine and subalpine grasslands and related communities
Hay meadows and fertilized pastures
Broad-leaved deciduous forests
Coniferous woodland
Mixed coniferous and deciduous forests
Fens, transition mires and springs
Screes
Inland cliffs and exposed rocks

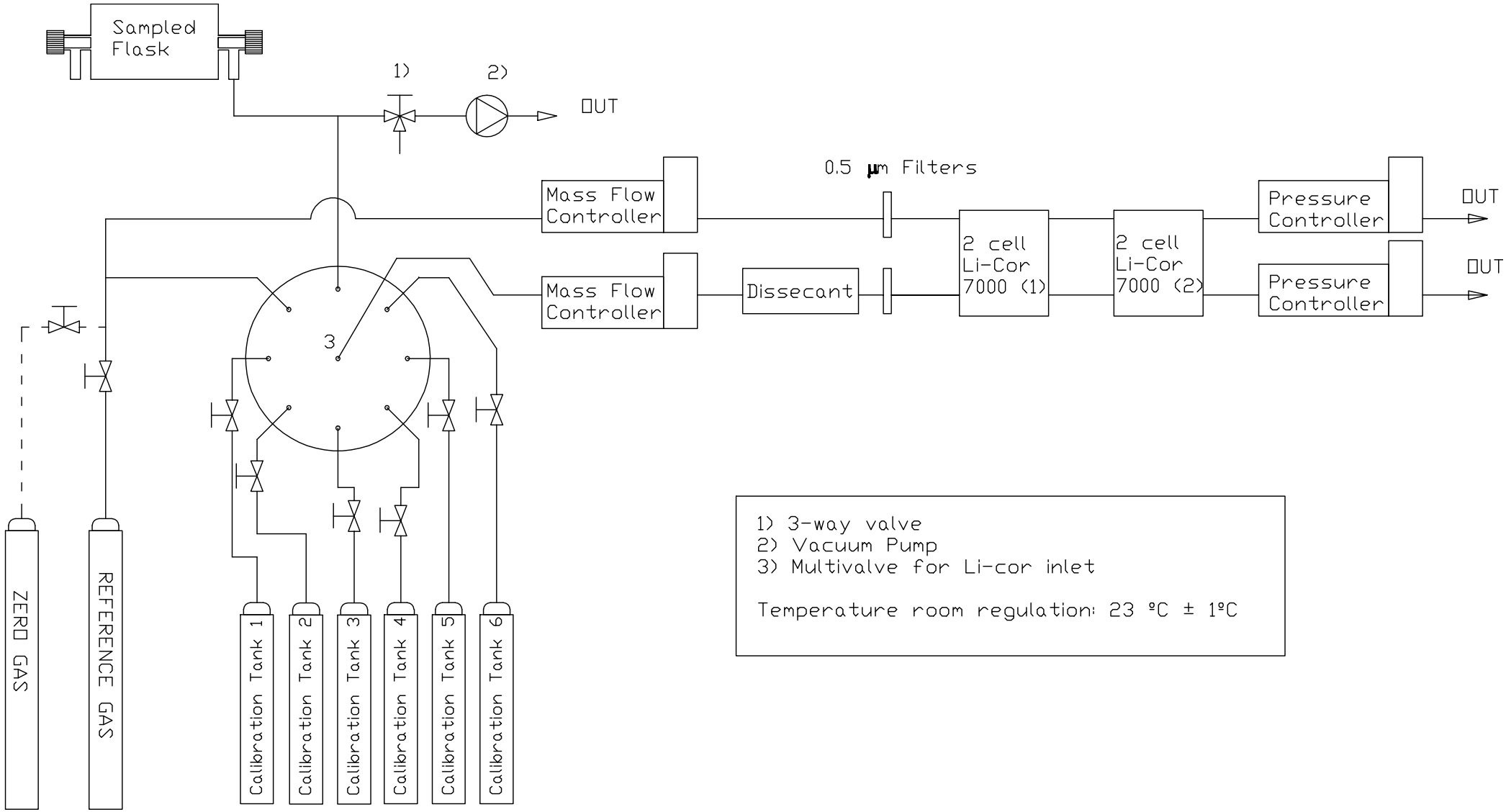
Sampled Flask
1)
2)
OUT
Mass Flow Controller
0.5 µm Filters
2 cell Li-Cor 7000 (1)
2 cell Li-Cor 7000 (2)
Pressure Controller
OUT
Mass Flow Controller
Dissecant
Pressure Controller
OUT
3
ZERO GAS
REFERENCE GAS
Calibration Tank 1
Calibration Tank 2
Calibration Tank 3
Calibration Tank 4
Calibration Tank 5
Calibration Tank 6
1) 3-way valve
2) Vacuum Pump
3) Multivalve for Li-cor inlet
Temperature room regulation: 23 ºC ± 1ºC

2010
2011
2012
2013
hour
month
CO_2 (ppm)
> 410
405
400
395
390
385
380
375